Supplementary data

High-Pressure Switch: Redirecting CO_2 Hydrogenation from Hydrocarbons to Carboxylic Acids and Alcohols

Jiyeon Lee[a,§], Muhammad Irshad[a,e,§], Wonjoong Yoon[a], Jaehoon Kim[a,b,c,d*]

[a] School of Chemical Engineering, Sungkyunkwan University,

2066, Seobu-Ro, Jangan-Gu, Sueon, Gyeong Gi-Do 16419, Republic of Korea

[b] School of Mechanical Engineering, Sungkyunkwan University,

2066, Seobu-Ro, Jangan-Gu, Suwon, Gyeong Gi-Do 16419, Republic of Korea

[c] SKKU Advanced Institute of Nanotechnology (SAINT), Sungkyunkwan University

2066, Seobu-Ro, Jangan-Gu, Suwon, Gyeong Gi-Do 16419, Republic of Korea

[d] Low-carbon Energy Engineering, Sungkyunkwan University

2066, Seobu-Ro, Jangan-Gu, Suwon, Gyeong Gi-Do 16419, Republic of Korea

[e] Center for Development, Demonstration and Training for Carbon-Free Technologies, National I nstitute of Chemistry, Hajdrihova 19, SI-1000 Ljubljana, Slovenia

[*] Corresponding author: jaehoonkim@skku.edu (Prof. Jaehoon Kim)

[§] Equally contributed

Table. S1. Summary of previously reported thermochemical CO_2 conversion studies using Fe-based catalysts under various reaction conditions.

Ref.	Catalyst	P (MPa)	T (°C)	Gas ratio (H_2/CO_2)	GHSV (mL g_{cat}^{-1} h^{-1})	TOS (h)	X_{CO2} (%)	Product selectivity without CO (%)				
								CO	CH_4	C_2-C_4 HCs	C_{5+} HCs	Oxygenates
[1]	Fe	5.0	320	2.8	24000	N.A.	13.6	14.2	46.8	36.0	11.4	5.8
[2]	$ZnFe_2O_4$	4.0	360	3	4000	8	48.2	8.9	5.8	22	72.2	N.A
[3]	Na-Fe_2O_3-900	3.5	330	3	4000	500	25.9	22.5	21.5	34.9	43.6	~10.0
[4]	Na-Fe_3O_4/HZSM-5	3.0	320	3	4000	N.A.	22.0	20.1	16.6	N.A.	31	13.0
[5]	Fe(12.9)	3.0	320	3	300	1	12.8	49.5	51.1	22.6	1.8	N.A
[6]	Fe	2.0	340	3	12000	N.A.	33.0	13.5	38.0	38.9	9.5	N.A
	FeMnNa	2.0	340	3	12000	N.A.	35.1	18.1	13.1	38.7	48.2	N.A
[7]	8.7nm Fe	1.1	300	3	4000	N.A.	35.0	15.1	14.3	54.0	31.7	N.A
[8]	FeCuNa	1.0	340	3	5000	50	40.1	4.9	11.2	35.6	53.2	N.A
[9]	0.09Mn/Fe_3O_4-NaAc	0.5	320	3	N.A.	10	27.6	24.7	12.8	44.8	42.4	N.A
[10]	Fe_3O_4-pur	0.5	300	3	2500	15	37.2	7.3	44.9	43.1	12.0	N.A
This study	**K-Fe_2O_3**	3.5	330	3	4000	100	38.6	14.7	14.7	42.3	41.0	2.3
		7.0	330	3	4000	100	22.6	19.2	25.3	55.8	8.9	10.0
		10.0	**330**	**3**	**4000**	**100**	**28.8**	**17.9**	**24.4**	**45.5**	**7.6**	**22.5**

[11]	FeK/Co-NC	2.5	300	3:1	4500	100	51.7	4.5	22.6	37.5	44.6	NA[b]
[12]	FeMnNa	2.0	340	3:1	12000	50	35.0	18.1	13.1	38.7	48.2	NA
[13]	$Na_{7.5}$-Fe-Co/ Al_2O_3	3.0	350	1:1	6000	100	32.8	8.1	13.7	37.4	48.9	NA
[14]	$ZnFeO_x$-2.68Na	3.0	320	3:1	4000	144	38.6	11.1	12.9	36.3	50.8	3.1
[15]	$FeAlO_x$-5	3.5	330	3:1	4000	50	36.8	7.2	12.1	30.1	57.8	0.7
		3.5	330	1:1	2000	450	18.9	28.9	5.3	16.4	74.1	3.2
[16]	R-Fe_5Zn_1	1.5	330	3:1	45000	200	34.8	9.4	13.9	31.5	54.6	<5.0
[17]	Fe-Mn-K	1.0	300	3:1	2400	80	38.2	5.6	10.4	27.7	61.9	NA
[18]	1Mn-Na/Fe	3.0	320	3:1	2040	10	39.3	9.0	8.1	28.2	54.4	NA
[19]	0.63%Na-Fe_2O_3	1.5	350	3:1	15000	50	41.0	15.5	14.1	30.9	51.8	NA
[20]	Na-$FeMgO_x$-5	3.5	330	3:1	4000	80	44.4	9.6	19.7	24.8	55.5	<5.0
[20]	Na-$FeMgO_x$-5	3.5	330	1:1	2000	680	19.6	25.4	6.7	26.8	66.5	7.0
[21]	C-2Fe-1Zn/K	2.0	320	3:1	1000	144	54.8	4.6	23.1	66.0	10.9	0.99
[22]	$CuFeO_2$	1.0	300	3:1	1800	15	17.3	31.7	2.7	31.0	66.3	NA
[23]	Na-$CoFe_2O_4$	3.0	320	3:1	7200	100	41.8	9.7	21.9	48.4	28.7	NA
[24]	1Fe-1Zn-K	0.5	300	3:1	1000	216	54.0	6.3	31.1	56.7	12.2	NA
[25]	Fe_5C_2-ZnO-3.0Na	1.5	320	3:1	10000	100	36.2	18.9	26.2	45.0	28.8	NA

[26]	10Mn-Fe_3O_4	2.0	350	3:1	4000	24	44.7	9.4	22.0	53.3	24.7	NA
[27]	FeNa	3.0	320	3:1	2000	100	40.5	13.5	15.8	54.1	30.1	NA
[28]	FeO_x-2	3.0	320	3:1	8000	50	34.1	12.6	13.0	40.3	46.7	NA
[29]	Fe/C-PYL	1.0	300	1:1	NA	6	21.6	29.2	36.8	46.0	17.2	NA
[30]	92.6Fe7.4K	2.5	300	3:1	560	NA	41.7	6.0	10.3	27.8	56.0	NA
[31]	Na-$FeZrO_x$-9	3.5	330	3:1	4000	50	44.0	6.8	14.0	27.4	58.5	4.2

[a] Oxygenated species and others
[b] Not available

Table S2. Metal contents of the catalysts as determined by ICP-OES analysis.

Catalyst	Metal contents (wt%)		Metal ratio
	K	Fe	[K/(K+Fe)] (%)
Calcined 3K-Fe_2O_3[a]	2.31	69.95	3.19
Reduced 3K-Fe_2O_3[b]	3.13	93.36	3.25
Spent KFe35[c]	1.63	37.56	4.15
Spent KFe70[c]	2.93	44.97	6.11
Spent KFe100[c]	1.96	56.91	3.33

[a] Calcination at 600 °C with a ramp rate of 1.6 °C min^{-1} for 6 h under static air
[b] Reduction at 350 °C and 3.5 MPa under H_2 flow (50 mL min^{-1}) for 12 h
[c] CO_2 hydrogenation at 330 °C, 0.1–10.0 MPa, H_2/CO_2 = 3, and GHSV = 6000 mL g^{-1} h^{-1} for 100 h.

Catalyst	BET surface area ($m^2\ g^{-1}$)	Pore volume ($cm^3 g^{-1}$)	Mean pore diameter (nm)	Crystallite size (nm)[d]
Calcined 3K-Fe_2O_3[a]	8.82	2.03	45.02	41.8
Reduced 3K-Fe_2O_3[b]	1.07	0.25	14.23	80.2
Spent KFe35[c]	0.19	0.85	13.63	57.0
Spent KFe70[c]	1.36	0.31	14.07	54.5
Spent KFe100[c]	1.17	0.27	17.20	49.2

Table S3. Textural properties and crystallite sizes of the 3K–Fe_2O_3 catalysts.

[a] Calcination at 600 °C with a ramp rate of 1.6 °C min^{-1} for 6 h under static air
[b] Reduction at 350 °C and 3.5 MPa under H_2 flow (50 mL min^{-1}) for 12 h
[c] CO_2 hydrogenation at 330 °C, 0.1–10.0 MPa, H_2/CO_2 = 3, and GHSV = 6000 mL g^{-1} h^{-1} for 100 h.
[d] Calculated from the full width at half maximum (FWHM) of Fe_2O_3(104), α-Fe(110) or Fe_3O_4 (311) for calcined, reduced and spent catalysts, respectively

Table S4. ^{57}Fe Mössbauer fitting parameters and corresponding phase compositions of the iron s pecies in the spent catalysts.

Catalyst	Phase	Fitting parameters			Spectral contribution (%)	
		H_{hf} (kOe)	δ (mm/s)	E_Q (mm/s)		
Spent KFe35	Fe_3O_4(I)	46.52	0.656	0.04	24.04	36.06
	Fe_3O_4(II)	49.97	0.308	0.01	12.02	
	Fe_5C_2(I)	21.92	0.243	0.09	23.88	60.47
	Fe_5C_2(II)	18.35	0.212	0.07	23.88	
	Fe_5C_2(III)	11.00	0.150	0.12	12.71	
	$FeCO_3$	-	1.240	1.90	1.22	1.22
	SPM	-	0.220	1.12	2.25	2.25
Spent KFe70	Fe_3O_4(I)	46.89	0.673	0.04	22.72	34.08
	Fe_3O_4(II)	50.00	0.286	0.01	11.36	
	Fe_5C_2(I)	22.02	0.243	0.10	22.05	55.83
	Fe_5C_2(II)	18.35	0.212	0.07	22.05	
	Fe_5C_2(III)	11.00	0.150	0.12	11.73	
	$FeCO_3$	-	1.233	1.90	6.52	6.52
	SPM	-	0.208	1.14	3.57	3.57
Spent KFe100	Fe_3O_4(I)	46.60	0.666	0.00	27.97	41.95
	Fe_3O_4(II)	50.00	0.296	0.00	13.98	
	Fe_5C_2(I)	22.00	0.240	0.09	16.37	41.97
	Fe_5C_2(II)	18.43	0.200	0.07	16.78	
	Fe_5C_2(III)	11.00	0.150	0.12	8.82	
	$FeCO_3$	-	1.252	1.86	11.18	11.18
	SPM	-	0.200	0.72	4.91	4.91

H_{hf}: Hyperfine magnetic field; δ: isomer shift (all the isomer shifts are referred to α-Fe foil at 298 K); E_Q: quadrupole splitting.

Table S5. Surface atomic composition of the catalysts as determined by XPS analysis.

Catalyst	Atomic compositions (%)			
	$C1_s$	$O1_s$	K_{2p}	Fe_{2p}
Calcined 3K-Fe_2O_3[a]	19.99	55.37	4.42	20.22
Reduced 3K-Fe_2O_3[b]	15.97	60.55	10.44	13.04
Spent KFe35[c]	66.23	26.81	3.13	3.84
Spent KFe70[c]	39.01	43.80	9.12	8.06
Spent KFe100[c]	30.15	48.91	10.61	10.32

[a] Calcination at 600 °C with a ramp rate of 1.6 °C min^{-1} for 6 h under static air
[b] Reduction at 350 °C and 3.5 MPa under H_2 flow (50 mL min^{-1}) for 12 h
[c] CO_2 hydrogenation at 330 °C, 0.1–10.0 MPa, H_2/CO_2 = 3, and GHSV = 6000 mL g^{-1} h^{-1} for 100 h.

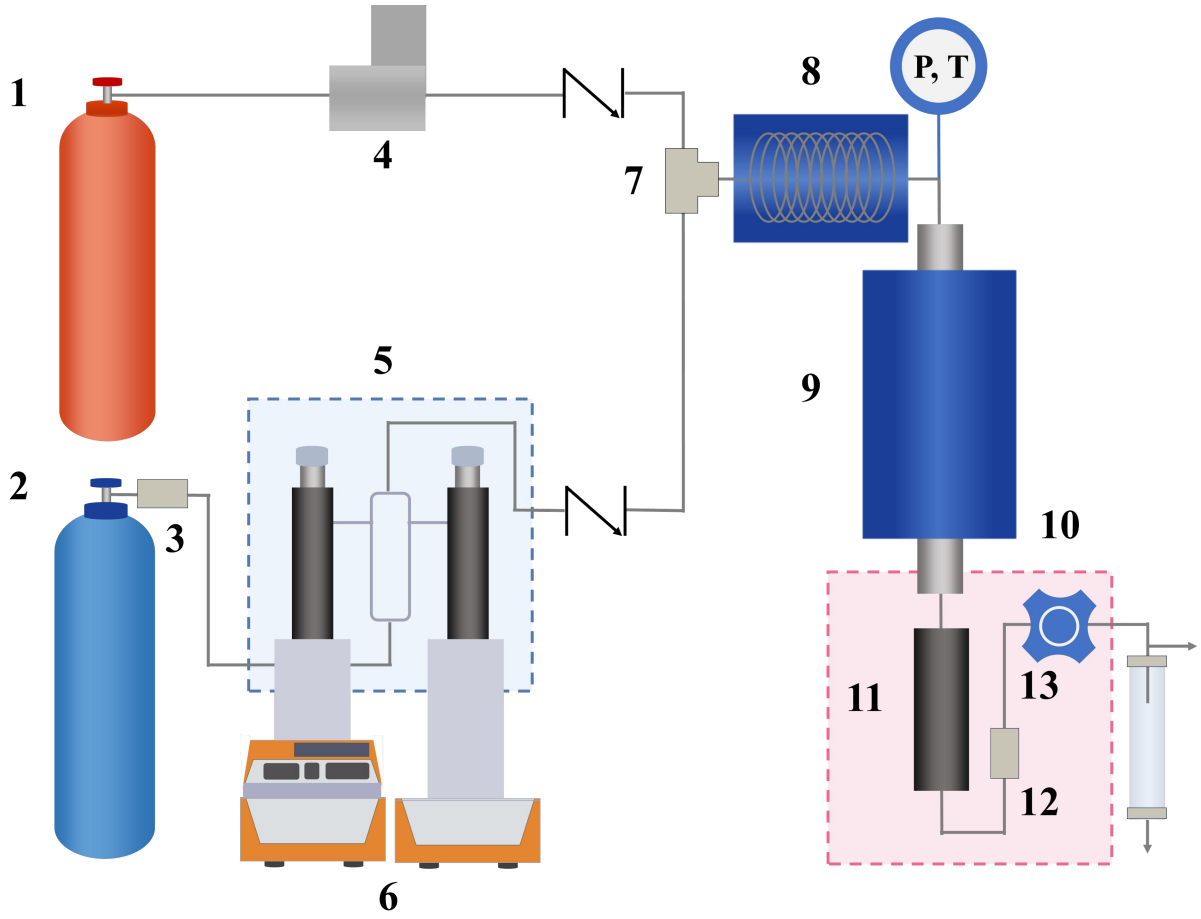

Fig. S1. Schematic diagram of the high-pressure continuous-flow CO_2 hydrogenation reactor system. 1—H_2 tank; 2—CO_2 tank with dip tube (siphon type); 3—Metal filter;4—H_2 mass flow controller (MFC); 5—Cooling circulator; 6—High-pressure syringe pump; 7—Mixing tee; 8—Pre-heater; 9—Fixed-bed tubular reactor; 10—Line heater; 11—Condenser; 12—Metal filter; 13—Back-pressure regulator (BPR).

H_2 was introduced into the reactor at a controlled flow rate using a mass flow controller (MFC; F-231M, Bronkhorst, USA). CO_2 was continuously supplied to the reactor using a high-pressure syringe pump (HP500x, ISCO, USA). To ensure a stable delivery of liquid CO_2 and prevent temperature fluctuations, the pump was maintained at 4 °C using a refrigerated bath circulator

(RW3-0525, JEIO Tech, Korea). Each feed line was equipped with a check valve to prevent backflow, and the H_2 and CO_2 streams were thoroughly mixed in a mixing tee before entering the reactor through a pre-heater maintained at 150 °C. The reactor temperature was monitored using a K-type thermocouple, and the system pressure was regulated by a back-pressure regulator (26-1762-24-043A, TESCOM, USA). Products exiting the fixed-bed reactor were condensed and subsequently analyzed in both the gas and liquid phases.

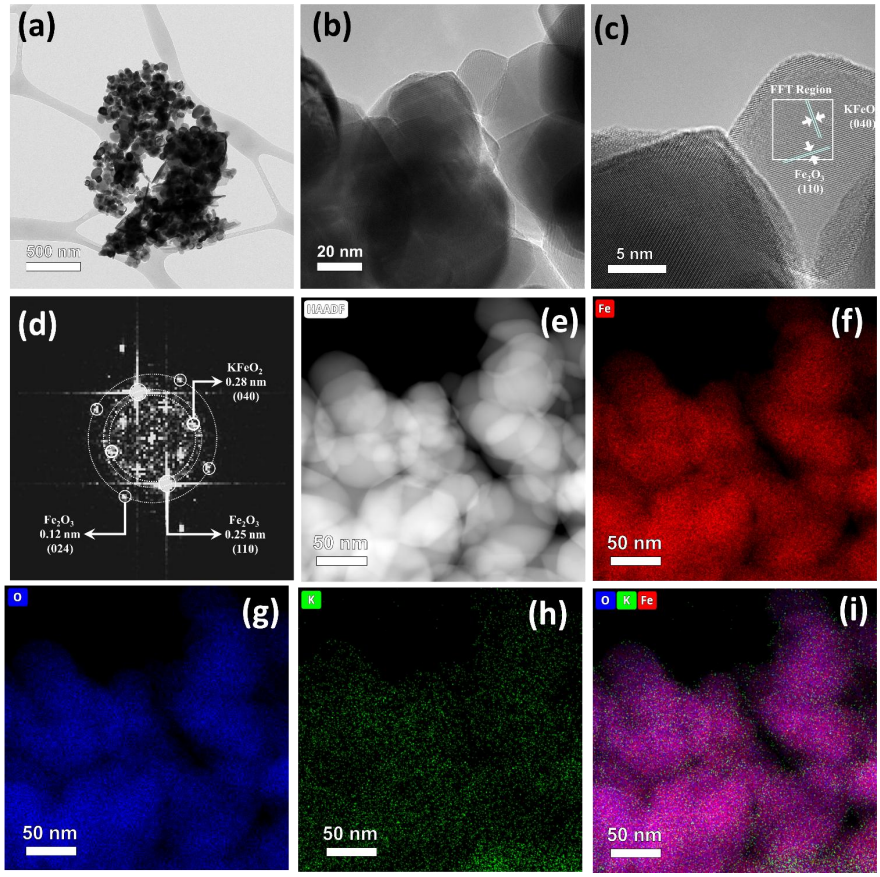

Fig. S2. Morphological and microstructural characterization of the calcined 3K–Fe_2O_3 catalyst. (a) Low-magnification TEM image showing aggregated oxide particles. (b) High-magnification TEM image revealing well-defined crystalline domains. (c) HR-TEM image with lattice fringes i ndexed to Fe_2O_3 (110) and $KFeO_2$ (040), confirming the coexistence of both phases. (d) Fast Fou rier transform (FFT) pattern corresponding to the region in (c), highlighting lattice spacings of Fe $_2O_3$ (024, 0.12 nm; 110, 0.25 nm) and $KFeO_2$ (040, 0.28 nm). (e) HAADF-STEM image of the sa me region. (f–h) EDS elemental maps showing the spatial distribution of Fe (red), O (blue), and K (green). (i) Composite EDS overlay map demonstrating the uniform dispersion of K and O ove r the Fe-containing oxide matrix.

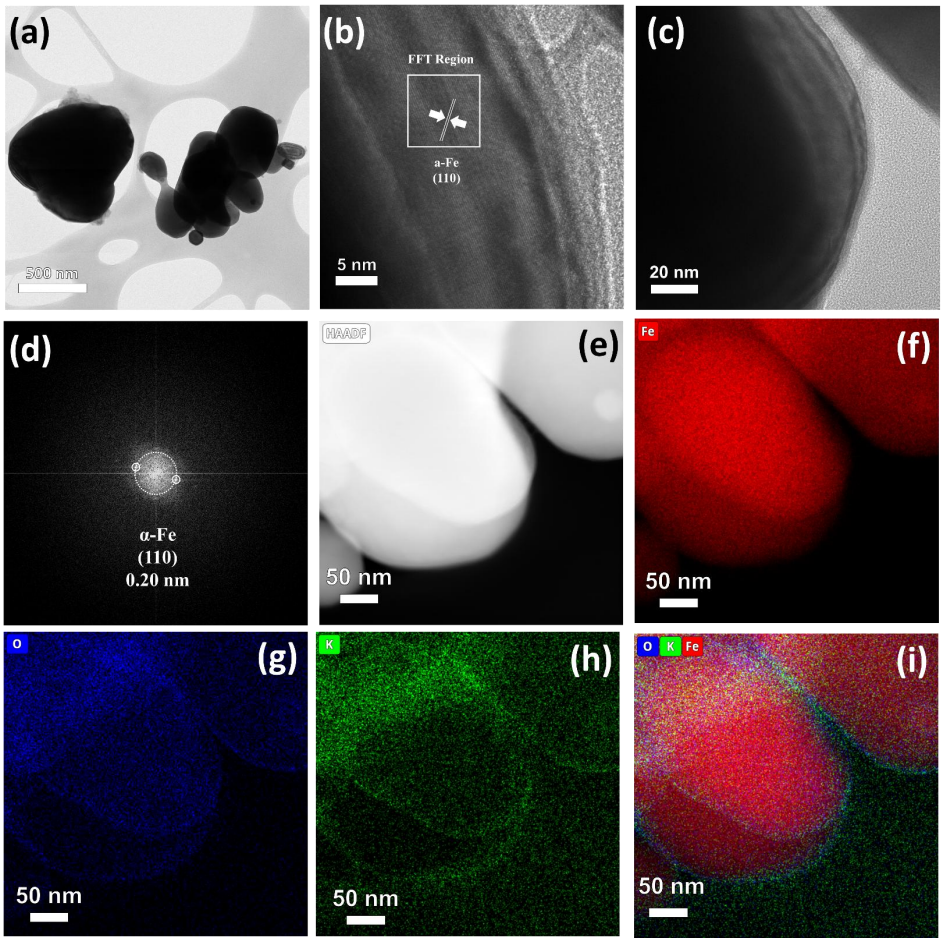

Fig. S3. Morphological and microstructural characterization of the H_2-reduced 3K–Fe_2O_3 catalyst. (a) Low-magnification TEM image showing the formation of large, sintered metallic particles after reduction. (b) HR-TEM image displaying lattice fringes assigned to α-Fe (110), confirming the presence of metallic iron. (c) HR-TEM image highlighting the smooth and densified particle surfaces induced by high-temperature reduction. (d) FFT pattern corresponding to the region in (b), showing the α-Fe (110) spacing (0.20 nm). (e) HAADF-STEM image of the reduced catalyst particles. (f–h) EDS elemental maps of Fe (red), O (blue), and K (green), respectively, illustrating the spatial distribution of elements after reduction. (i) Composite EDS overlay map demonstrating uniform but surface-localized potassium dispersion over the metallic Fe domains.

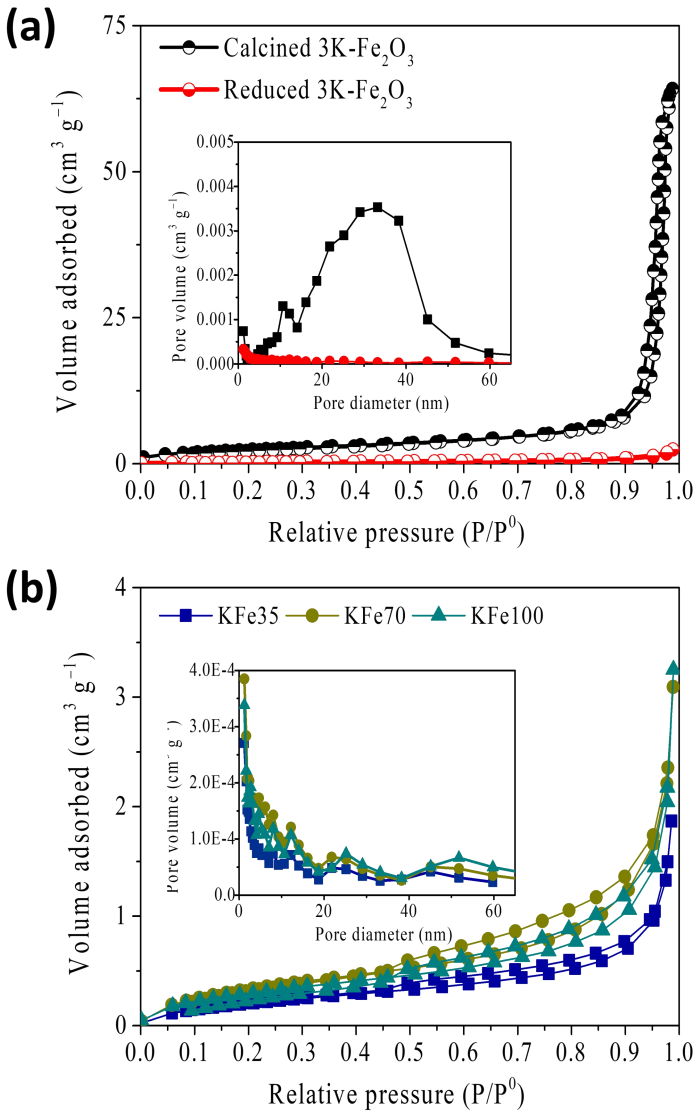

Fig. S4. N_2 adsorption–desorption isotherms and corresponding BJH pore-size distributions for (a) and (b) the calcined and H_2-reduced 3K–Fe_2O_3 catalysts, and (c) the spent catalysts obtained after CO_2 hydrogenation at their respective reaction pressures.

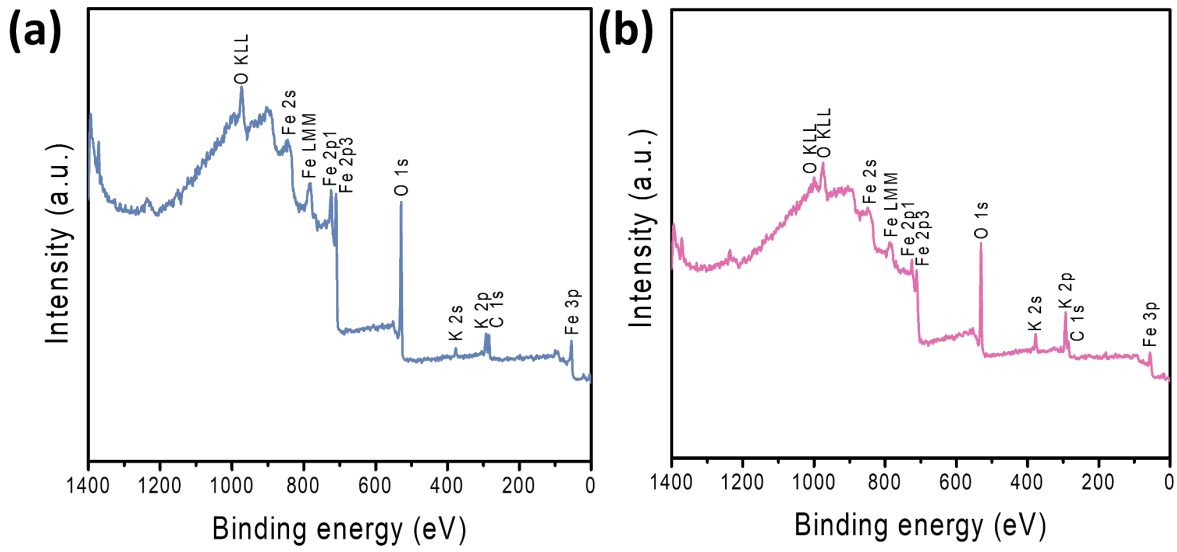

Fig. S5. XPS survey (wide-scan) spectra of the 3K–Fe_2O_3 catalyst in its (a) calcined and (b) H_2-reduced states prior to CO_2 hydrogenation.

References

[1] H. Zhao, L. Guo, W. Gao, F. Chen, X. Wu, K. Wang, Y. He, P. Zhang, G. Yang, N. Tsubaki, *J. CO2 Util.*, **2021**, 52, 101700.

[2] L. Zhang, J. Zhao, T. Li, W. Gao, H. Li, L. Wu, W. Xia, W. Wu, C. Wang, F. Wang, *Nano Lett.*, **2025**, 25, 4904-4912.

[3] S. Ahmed, W. Yoon, H. Jo, M. Irshad, M. K. Khan, J. Kim, *Chem. Eng. J.*, **2024**, 499, 156104.

[4] J. Wei, Q. Ge, R. Yao, Z. Wen, C. Fang, L. Guo, H. Xu, J. Sun, *Nat. Commun.*, **2017**, 8, 15174.

[5] J. Zhu, G. Zhang, W. Li, X. Zhang, F. Ding, C. Song, X. Guo, *ACS Catal.*, **2020**, 10, 7424-7433.

[6] Y. Xu, P. Zhai, Y. Deng, J. Xie, X. Liu, S. Wang, D. Ma, *Angew. Chem.*, **2020**, 132, 21920-21928.

[7] W. Meng, B. C. de Jong, H. van de Bovenkamp, G.-J. Boer, G. L. Bezemer, A. I. Dugulan, J. Xie, *Chem. Eng. J.*, **2024**, 489, 151166.

[8] Y. Liu, X.-a. Pan, Z. Qiu, L. Sun, P. Zhang, R. He, Z. Han, J. Chen, S. Liu, H. Wei, *Fuel*, **2025**, 393, 135036.

[9] B. Liu, S. Geng, J. Zheng, X. Jia, F. Jiang, X. Liu, *ChemCatChem*, **2018**, 10, 4718-4732.

[10] Z. Sun, X. Chen, F. Lu, L. Zhou, Y. Zhang, *Catal. Commun.*, **2022**, 162, 106387.

[11] S.-M. Hwang, S. J. Han, H.-G. Park, H. Lee, K. An, K.-W. Jun, S. K. Kim, *ACS Catal.*, **2021**, 11, 2267-2278.

[12] Y. Xu, P. Zhai, Y. Deng, J. Xie, X. Liu, S. Wang, D. Ma, *Angew. Chem., Int. Ed.* , **2020**, 132, 21920-21928.

[13] C. Dai, X. Zhao, B. Hu, X. Zhang, Q. Luo, X. Guo, X. Ma, *J. CO2 Util.*, **2021**, 43, 101369.

[14] X. Cui, P. Gao, S. Li, C. Yang, Z. Liu, H. Wang, L. Zhong, Y. Sun, *ACS Catal.*, **2019**, 9, 3866-3876.

[15] M. K. Khan, P. Butolia, H. Jo, M. Irshad, D. Han, K.-W. Nam, J. Kim, *ACS Catal.*, **2020**, 10, 10325-10338.

[16] C. Zhang, C. Cao, Y. Zhang, X. Liu, J. Xu, M. Zhu, W. Tu, Y.-F. Han, *ACS Catal.*, **2021**, 11, 2121-2133.

[17] B. Yao, T. Xiao, O. A. Makgae, X. Jie, S. Gonzalez-Cortes, S. Guan, A. I. Kirkland, J. R. Dilworth, H. A. Al-Megren, S. M. Alshihri, *Nat. Commun.*, **2020**, 11, 1-12.

[18] B. Liang, T. Sun, J. Ma, H. Duan, L. Li, X. Yang, Y. Zhang, X. Su, Y. Huang, T. Zhang, *Catal. Sci. Technol.*, **2019**, 9, 456-464.

[19] X. Liu, C. Zhang, P. Tian, M. Xu, C. Cao, Z. Yang, M. Zhu, J. Xu, *J. Phys. Chem. C*, **2021**, 125, 7637-7646.

[20] S. Ahmed, M. Irshad, W. Yoon, N. Karanwal, J. R. Sugiarto, M. K. Khan, S. K. Kim, J. Kim, *Appl. Catal. B: Environ.*, **2023**, 123052.

[21] X. Wang, J. Zhang, J. Chen, Q. Ma, S. Fan, T.-s. Zhao, *Chin. J. Chem. Eng.*, **2018**, 26, 761-767.

[22] Y. H. Choi, Y. J. Jang, H. Park, W. Y. Kim, Y. H. Lee, S. H. Choi, J. S. Lee, *Appl. Catal. B: Environ.*, **2017**, 202, 605-610.

[23] F. Yuan, G. Zhang, J. Zhu, F. Ding, A. Zhang, C. Song, X. Guo, *Catal. Today*, **2021**, 371, 142-149.

[24] J. Zhang, S. Lu, X. Su, S. Fan, Q. Ma, T. Zhao, *J. CO2 Util.*, **2015**, 12, 95-100.

[25] W. Tu, C. Sun, Z. Zhang, W. Liu, H. S. Malhi, W. Ma, M. Zhu, Y.-F. Han, *Appl. Catal. B: Environ.*, **2021**, 298, 120567.

[26] J. Jiang, C. Wen, Z. Tian, Y. Wang, Y. Zhai, L. Chen, Y. Li, Q. Liu, C. Wang, L. Ma, *Ind. Eng. Chem. Res.*, **2020**, 59, 2155-2162.

[27] J. Wei, J. Sun, Z. Wen, C. Fang, Q. Ge, H. Xu, *Catal. Sci. Technol.*, **2016**, 6, 4786-4793.

[28] R. Yao, J. Wei, Q. Ge, J. Xu, Y. Han, H. Xu, J. Sun, *Catal. Today*, **2021**, 371, 134-141.

[29] L. Guo, P. Zhang, Y. Cui, G. Liu, J. Wu, G. Yang, Y. Yoneyama, N. Tsubaki, *ACS Sustain. Chem. Eng.* , **2019**, 7, 8331-8339.

[30] S. Geng, F. Jiang, Y. Xu, X. Liu, *ChemCatChem*, **2016**, 8, 1303-1307.

[31] S. Ahmed, J. R. Sugiarto, W. Yoon, M. Irshad, H. Jo, S. S. Bibi, S. K. Kim, M. K. Khan, J. Kim, *J. Energy Chem.*, **2025**, 102, 431-442.